Separation control of a NACA 4412 with 25° sweep at high Reynolds numbers using pulsed-jet actuators

Pierre-Yves Passaggia, Stéphane Loyer, Azeddine Kourta, Lucien Baldas, Stéphane Orieux, Phassawat Leelaburanathanakul, Guillermo Lopez Quesada, Christine Barrot-Lattes, Ahmad Batikh, Nicolas Mazellier

Association Aéronautique et Astronautique de France

58th 3AF International Conference on Applied Aerodynamics
27 — 29 March 2024, Orléans – France

AERO2024-0038

Separation control of a NACA 4412 with 25^o sweep at high Reynolds numbers using pulsed-jet actuators

P.-Y. Passaggia[(1)], S. Loyer[(1)], A. Kourta[(1)], L. Baldas[(2)], S. Orieux[(2)], P. Leelaburanathanakul[(2)], G. Lopez-Quesada[(2)], C. Barrot-Lattes[(2)], A. Batikh[(2)], N. Mazellier[(1)]

[(1)] *University of Orléans, INSA-CVL, PRISME, EA 4229, 45072 Orléans, France*

pierre-yves.passaggia@univ-orleans.fr

[(2)] *Institut Clément Ader (ICA), Université de Toulouse, CNRS, INSA, ISAE-SUPAERO, Mines-Albi, UPS, Toulouse, France*

ABSTRACT

Boundary-layer separation at large Reynolds numbers over swept wings remains a challenging phenomenon to either replicate in well-controlled laboratory experiments or predict in full-scale applications. The present work reports the aerodynamic performances of a wind-tunnel model based on a NACA 4412 airfoil with a sweep angle of 25° at Reynolds number up to 10^6. In addition, A flow-control strategy based on bi-stable fluidic oscillators is presented where the pulsed jet actuators (PJA) are capable of reaching frequencies of several kHz. This novel setup aims at improving the authority of the control while minimising the power input by the actuators. To this end, several actuators were designed and tested to determine the best configuration. In this paper, we provide a summary of the results obtained for the best actuator and demonstrate net gains as high as 18% near stall, for values of the momentum coefficient as low as 2.5×10^{-4}. The success behind this strategy resides in the low-speed high-mass-flow-rate provided by the design of the actuators which compensate for the mass and momentum deficits in the boundary layer and delay efficiently separation. This study underlines the potential for upscaling this strategy to the full scale where the flow injected for the control is generally limited.

1. EXPERIMENTAL CHARACTERISATION OF THE WIND-TUNNEL MODEL

Experiments were carried out in the S1 wind tunnel at PRISME laboratory (Orléans, France). The test section of this closed-loop wind tunnel is a 2×2 m^2 square, extending over 5 m. The airfoil model is a NACA 4412 with a sweep angle $\beta = 25°$ and a constant chord $c =$ 300 mm along the wingspan. In this study, the wind speed U_∞ was set to 50 m/s, which leads to chord-based Reynolds number $Re_c = U_\infty c/\nu$ (with ν the kinematic viscosity of air) up to 10^6. To mitigate the interference with the boundary layers developing along the wind tunnel walls, the airfoil model has been set between two side walls installed within the test section as illustrated in Fig. 1. The distance between the side walls is 1100 mm leading to an airfoil aspect ratio of $AR \approx 3.7$. Furthermore, the laminar-to-turbulent boundary layer transition on the airfoil is triggered by employing zig-zag turbulators (0.4 mm thick) located at 7% of the chord from the leading edge on both suction and pressure sides. The airfoil is clamped on two discs equipped with two independent rotation stages enabling the variation of the angle of attack AoA over the range $[0°, 20°]$ and compensating for hysteresis due to model twist. The investigated free-stream velocity, monitored by a Pitot probe located at 1 m from the beginning of the straighteners, is $U_\infty \pm 1.5\%$ m/s. The static pressure tap of the Pitot tube is used as a reference pressure p_∞. The aerodynamic loads experienced by the model are measured through a 6-component balance. In addition, 156 pressure taps are used to investigate the pressure distribution around the airfoil.

The lift coefficient $C_L = 2L/\rho S U_\infty^2$ is computed using both the force balance and the integration of the pressure coefficient $C_p \equiv 2(p - p_\infty)/\rho U_\infty^2$ along the chord at the mid span (see Figs. 2(a) and 2(b)). Here ρ is the density of the fluid, S is the surface area, while L and D are the lift and drag forces measured by the force balance. Our results are compared to those from [1] who performed measurements on an unswept NACA 4412 (i.e. $\beta = 0$)

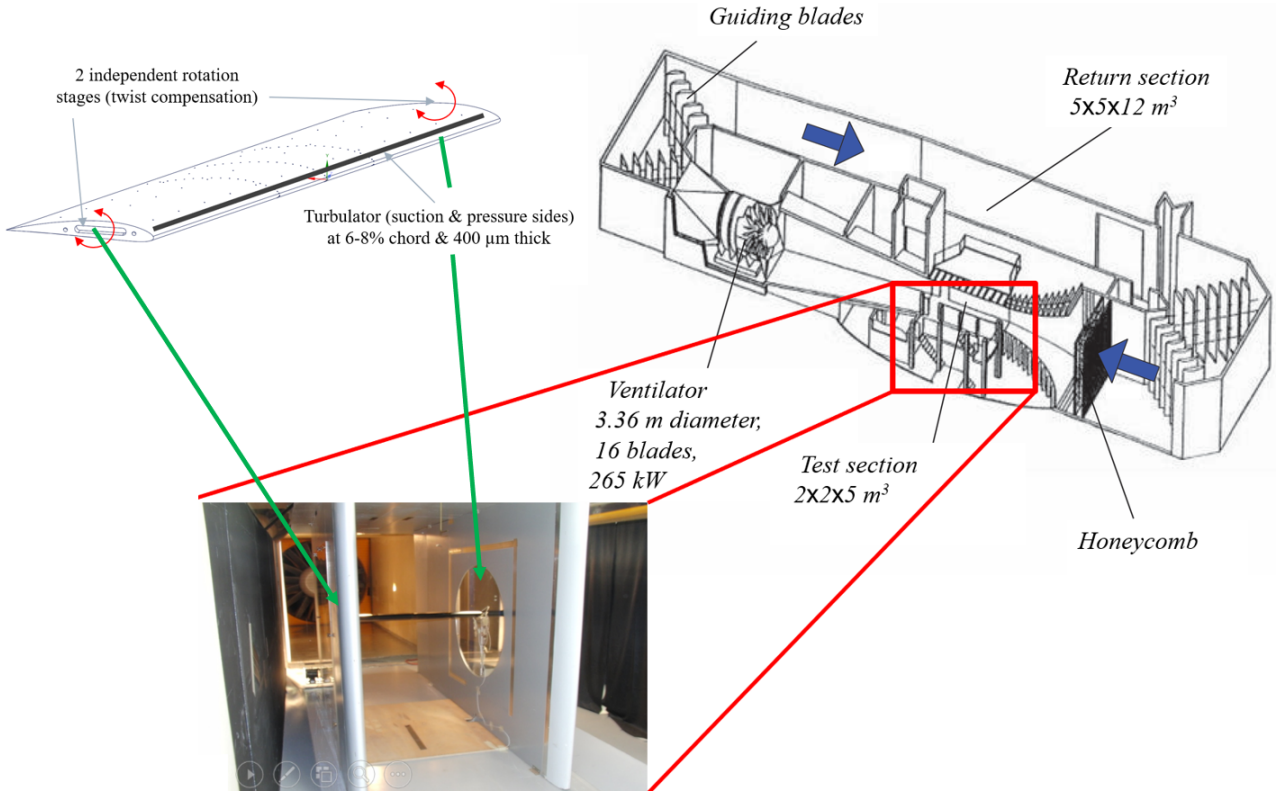

Figure 1: Sketch of the wind tunnel, the test section, and the model.

and the recent Large Eddy Simulation (LES) reported in [4] for the same flow geometry and at an angle of attack $AoA = 5°$. Note that both measurements from [1] and [4] were corrected with the sweep angle (i.e. multiplied by $\cos(\beta)$). Lift coefficient values are in good agreement as far as 3D effects induced by the swept geometry remain marginal. Note that the LES predicts a lift coefficient slightly higher than that observed experimentally, which may be due to the finite size effect in experiments. Note that separation occurs earlier than for the case of the unswept airfoil model which triggers separation for a larger AoA.

2. FLUIDIC OSCILLATORS

The PJAs introduced in this work are based on fluidic oscillators [5] with some modifications to make them suitable for integration in the NACA4412 airfoil. These new PJAs consist of one inlet nozzle connected to a switching zone that is divided into two long channels by a splitter, each of them leading towards a feedback loop. These feedback loops reconnect to the switching zone through their respective control ports. At the beginning of each feedback loop, an elbow connects with a reservoir and the outlet channels (see figure 3(a,b)).

The oscillatory behaviour of the actuator is provided by the feedback-loop geometry and the control ports connected to the switching zone. Considering for example an initial flow from the inlet nozzle attached, thanks to the Coanda effect, to the splitter channel, part of the flow would exit from the actuator through the outlet while the rest of the flow would run along the feedback loop and its corresponding control port, increasing the pressure in this loop with a compression wave propagating roughly at the speed of sound c_0. The main control parameter for the frequency f of oscillation is typically the length l_f of the feedback loop through the following expression $f = c_0/4l_f$ [5]. Since the objective is to allow flow control along the span of the wing, a large assembly of oscillators is required. If the oscillators were left independent from each other, their oscillatory frequencies could vary or have different phases due to manufacturing imperfections or variations in the operating conditions. However, the proposed design allows for a natural synchronisation of the assembly by connecting the feedback loops of any oscillator with the control port of the adjacent ones. The most sensitive region to the actuation of the flow is located on the first half of the suction side. The typical dimensions of the experimental airfoil result in a very limited space for the implementation of the PJAs inside the airfoil. The PJA assembly is designed accordingly in three different positions for the actuation that are proposed to be evaluated in the chord-like direction (5%, 10%, and 15% of the chord length). To obtain

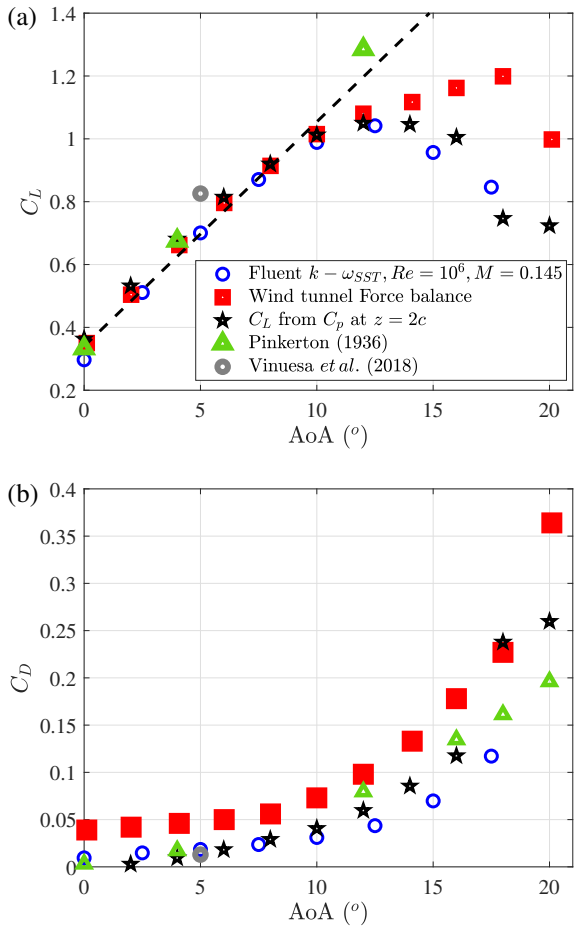

Figure 2: Comparison between (a) the lift coefficient and (b) the drag coefficient between the force balance (red squares) and the integration of the pressure coefficient (black pentagrams) computed at the mid-span. The grey dot reports the values from the high-fidelity numerical simulation [4] and the green triangles correspond to the experiment from [1]. The blue dots report the results from the numerical simulations. Note that both results from [4, 1] were corrected using the sweep angle for consistency.

suitable frequencies (of the order of 1 kHz) for the separation control theoretically requires feedback loop lengths longer than 100 mm. Since the space allocated for the feedback loops is very limited due to the geometrical constraints, modifications to the internal design of previous fluidic oscillators found in the literature are required. The numerical investigation has been then focused on reducing the frequency for shorter feedback loops by modifying the splitter area of the oscillator as well as increasing the complexity of the feedback loop while keeping a proper switching of the jet. The numerical investigation was performed with ANSYS Fluent using a coupled solver, second-order discretization scheme and the realisable $k-\varepsilon$ turbulent model. Several 3D models of at least 2 synchronised oscillators (2 inlets, 4 outlets) have been simulated. The numerical study was focused on characterising the outlet jet velocities and the frequency of oscillation (Fig. 3(c)).

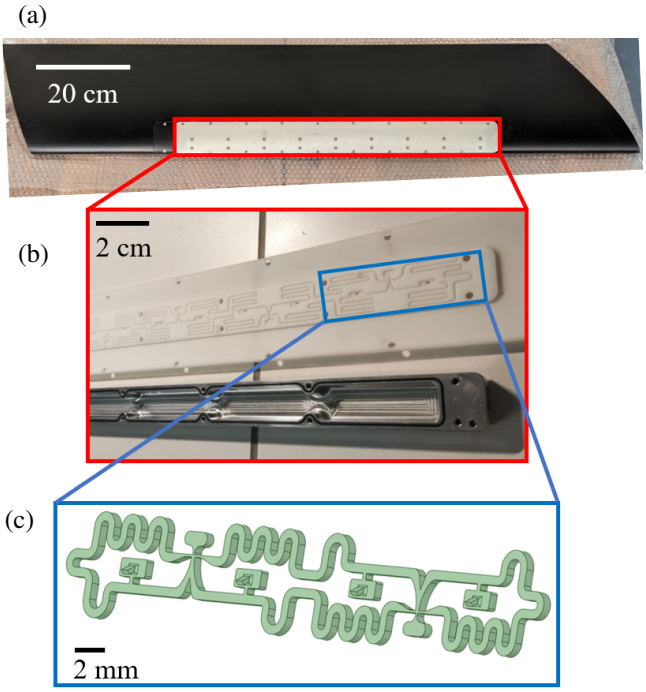

Figure 3: (a) Wing-tunnel model equipped with the pulsed-jet actuator, (b) 3D printed sample of a pulsed-jet-actuator assembly together with the reservoir design, (c) design of the feedback loop length of 137mm.

Next, actuators are characterized using hot-wire anemometry over the entire span of the actuator to determine the angle of injection, the homogeneity of the velocity outlet and the frequency for each actuator. Figure 4(a) shows the time-averaged modulus of the mean velocity further averaged over the top of each outlet. Tracing the maximum velocity for each streamwise position, the mean angle of injection of the PJA is measured near 22^O without free-stream velocity. Further test benches were carried out such as measurements of the maximum velocity above each PJA along the span of the actuator. Figure 4(b) shows this evolution for the six actuators (12 outlets) and along the full span of the actuator ranging from $z/c = [-0.8, 0.8]$. The frequency for each actuator (not shown here) was also measured and provided results in the range $f_{act} \approx 1047 \pm 20$ Hz which corresponds to a Strouhal number $St = fc/U_\infty \approx 7$ for the actuators. Although the density of the air exiting at these locations differs from the one used for the calibration, these measurements confirm the homogeneity and thereby the quality of the fabrication process along the different spanwise loca-

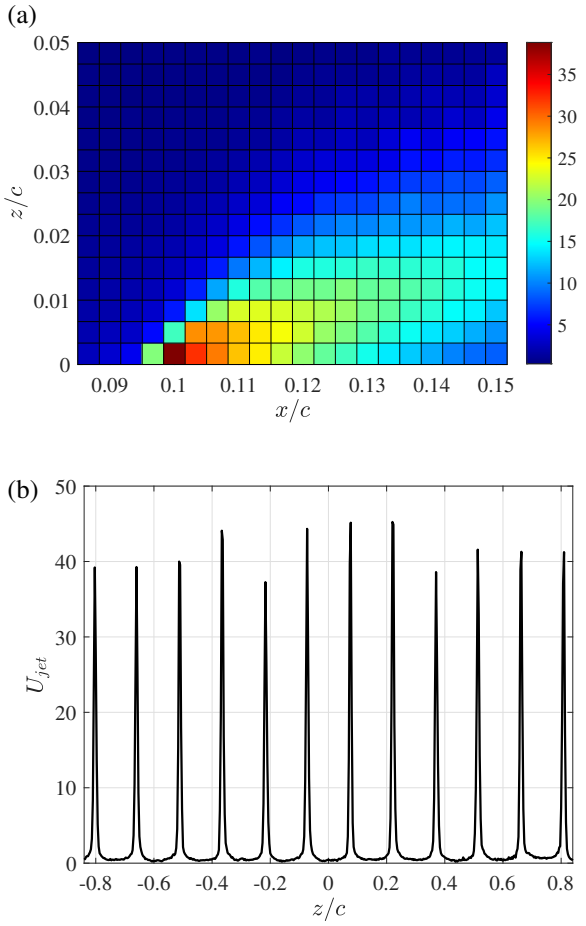

Figure 4: Bench tests of (a) mean absolute value of the velocity measured by the hot wire averaged over all actuators. (b) Measurement of the maximum PJA velocity along the span at $x/c \approx 0.1$.

tions demonstrating the feasibility of the design, even for such a scaled model.

3. WIND-TUNNEL TESTING WITH PULSED-JET ACTUATORS

The next part investigates the effect of the active-flow control using the pulsed-jet actuators at different flow rates on the aerodynamic performances of the airfoil taking as a reference, the results reported in this abstract. Experiments were carried out at a free-stream velocity $U_\infty \approx 50$ m/s which provided a Reynolds number $Re \approx 10^6$ for the results summarised in this paper. For each experiment, measurements of the temperature and the pressure in both the wind tunnel and the reservoir of the actuator allowed for monitoring the evolution of the different aerodynamics and control coefficients carefully.

In what follows, we define the momentum coefficient as $C_\mu = \rho_{act} U_{act} \dot{V}_{act} / \rho_\infty U_\infty^2 S$ where U_{act} is the "true" velocity at the outlet of the actuator and $\dot{V}_{act}$ is the volume-flow rate measured by the solenoid valve. The latter reached up to 240 nl/min.

The velocity and the density of the actuator were estimated using the inviscid compressible nozzle analogy for the different pressures and temperatures supplied in the tank. In these experiments, it is worth mentioning that once the flow becomes sonic at the throat of the actuator, increasing the pressure in the reservoir no longer increases the velocity at the outlets nor changes the frequency of the actuators. The only quantity which turns out to be modified is the density of the actuators ρ_{act} which evolves linearly with C_μ. While the momentum coefficient measures the ratio of momentum injected compared to the momentum produced by the wind tunnel, another metric has to be defined to determine the net mean aerodynamic gain obtained by the control. This can be achieved using the Aerodynamic Figure of Merit (AFM) defined in [2] as

$$AFM = \frac{C_L/(C_D + C_{pow})}{C_{L|_{C_\mu=0}}/C_{D|_{C_\mu=0}}},$$

which measures the net aerodynamic gain comparing the power obtained from the wing, amended by the power used by the control defined as

$$C_{pow} = \dot{V}_{act} \left(P_{tot,act} - P_{act}\right) / (\rho_\infty U_\infty^3 S)$$

where ($P_{tot,act}$ is the total pressure while P_{act} designates the static pressure, both measured in the actuator.

Results for the mean aerodynamics coefficients as well as the aerodynamic figure of Merit are reported in Figure 5 for this particular actuator. For nearly all angles of attack, the actuator improves the lift (increase) and the drag (decrease) coefficients and this improvement follows with the increase of the momentum coefficient C_μ. The drag and the lift are both improved by nearly 10%, for the largest value of the actuation and close to separation, whose onset is observed at $AoA \approx 18^o$. Although separation is not delayed, it is worth mentioning that the momentum coefficient is of the order of 10^{-4} which is extremely low. This is particularly important, especially when analysing the aerodynamic figure of merit, shown in figure 5(c). The largest value of C_μ that could be attained in this experiment allows for attaining $AFM \approx 1.18$, corresponding to an 18% net improvement at $AoA = 17.5$ and $Re \approx 10^6$.

To further understand how the flow responded to the pulsed-jet actuator, Stereo Particle-Image Velocimetry (SPIV) was performed right before separation occurred. Results are reported in figure 6(a) for the natural case while the best control case is shown in figure 6(b) at $AoA = 17.75^o$. In these figures, mean streamlines are represented in white and superimposed on colour maps of the

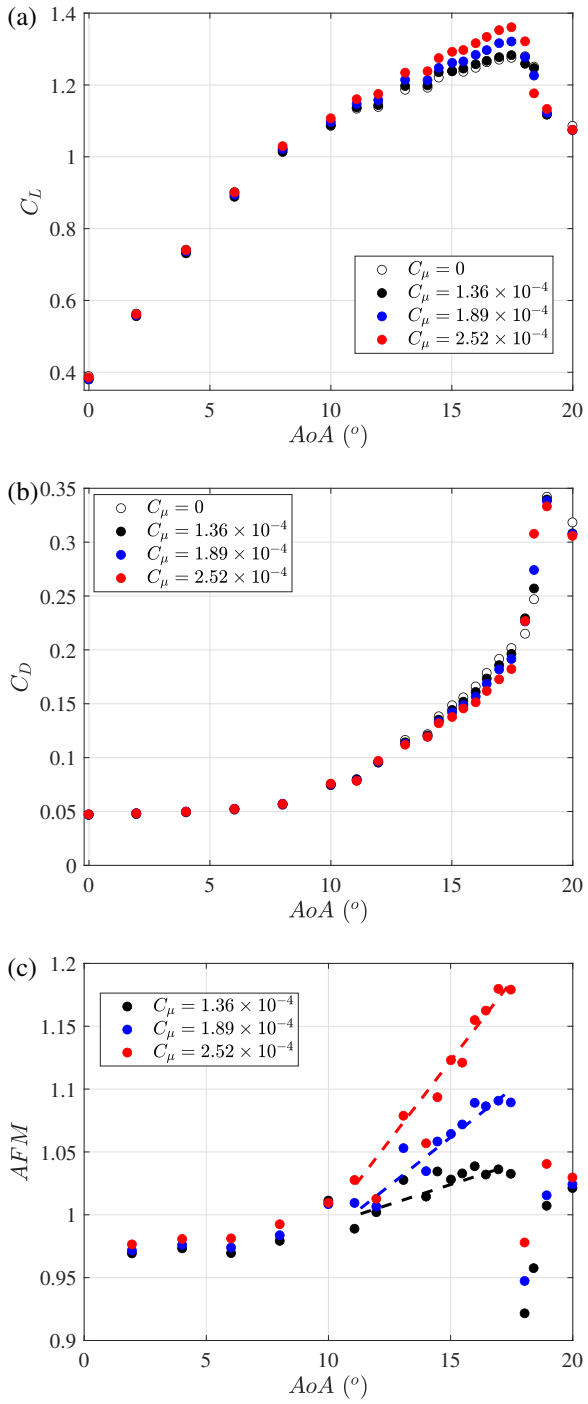

Figure 5: Comparison between (a) the lift coefficient and (b) the drag coefficient obtained from the force balance at $Re = 10^6$ as a function of the angle of attack AoA for three different values of C_μ. (c) The aerodynamic figure of merit shows the net gain obtained by the control for the three cases presented above.

turbulent kinetic energy. The net aerodynamic gain is visible and the PJA delays separation from the leading edge

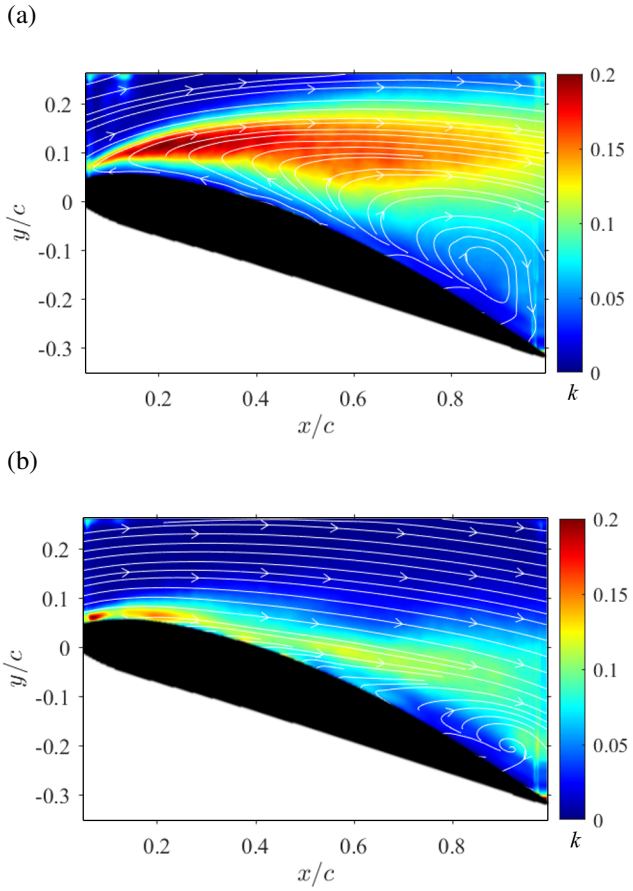

Figure 6: Mean SPIV measurements (white streamlines) and turbulent kinetic energy (colour map) for (a) the natural case and (b) the controlled case at $C_\mu = 2.52 \times 10^{-4}$, $Re = 10^6$, and $AoA = 17.75^o$. showing the effect of the control.

until $x/c \approx 0.55$. The large recirculation region for the natural case is reduced to an incipient separation zone displaying reduced levels of turbulent kinetic energy. This analysis suggests that the net aerodynamic gain might be spanwise dependent and a deeper analysis will be carried out during the presentation where a full local budget will be proposed using these SPIV measurements, combined with local static pressure measurements obtained using the pressure scanner [3].

4. CONCLUSION

This study provides the main characteristics for the design and validation of a flow-control strategy for pulsed-jet actuators integrated into a wind tunnel model and tested at high Reynolds numbers. The present model, a 2.5D NACA 4412 aerofoil with a 25^o sweep angle, is first validated against numerical simulations and the existing literature for the same geometry. Although the present

work considered a large range of actuator designs, results for the characterisation and the validation against numerical simulations of the best actuator are provided. Although the momentum injected for the control is four orders of magnitude smaller than the momentum generated by the lift of the wing, the present study shows that pulsed-jet actuators can improve the aerodynamics coefficient, the measure of which is provided by the aerodynamic figure of merit which reports 18% net gains for the best case, based on the lift-to-drag coefficient. However, particle-image velocimetry reveals that this gain might be even larger when only considering the central section of the airfoil. This analysis will be further detailed during the conference, coupling local pressure measurements with pressure reconstruction using mean particle-image velocimetry measurements [3].

Acknowledgements

This project has received funding from the Clean Sky 2 Joint Undertaking (JU) under grant agreement No 887010. The JU receives support from the European Union's Horizon 2020 research and innovation programme and the Clean Sky 2 JU members other than the Union.

REFERENCES

[1] R. M. Pinkerton. *Calculated and measured pressure distributions over the midspan section of the NACA 4412 airfoil*, volume 563. NACA T. R., 1936.

[2] A Seifert. Closed-loop active flow control systems: actuators. In *Active Flow Control: Papers contributed to the Conference "Active Flow Control 2006", Berlin, Germany, September 27 to 29, 2006*, pages 85–102. Springer, 2007.

[3] R. Shanmughan, P.-Y. Passaggia, N. Mazellier, and A. Kourta. Optimal pressure reconstruction based on planar particle image velocimetry and sparse sensor measurements. *Exp. Fluids*, 61:1–19, 2020.

[4] R. Vinuesa, P. S. Negi, M. Atzori, A. Hanifi, D. S. Henningson, and P. Schlatter. Turbulent boundary layers around wing sections up to rec= 1,000,000. *Int. J. Heat & Fluid Flow*, 72:86–99, 2018.

[5] S. Wang, A. Batikh, L. Baldas, A. Kourta, N. Mazellier, S. Colin, and S. Orieux. On the modelling of the switching mechanisms of a Coanda fluidic oscillator. *Sens. & Actuat. A: Phys.* , 299:111618, November 2019.